JOURNAL OF THERMOPHYSICS AND HEAT TRANSFER
Vol. 24, No. 3, July–September 2010

Geometric Effects on Critical Heat Flux on Horizontal Microporous Coatings

Chen Li*
University of South Carolina, Columbia, South Carolina, 29208
and
G. P. Peterson†
Georgia Institute of Technology, Atlanta, Georgia, 30332

DOI: 10.2514/1.37619

This study aims to understand the effects of the geometric parameters of microporous coatings on the critical heat flux through systematic series of experimental studies. The test results indicated that critical heat flux of microporous coated surfaces is strongly dependent on the coating thickness, volumetric porosity, and pore size. For a given heating area, the critical heat flux mechanism was found to be distinguished by the microporous coating thickness. In addition, the optimal volumetric porosity was found to exist when the mesh size and coating thickness were held nearly constant. The wire diameter was found to play an important role in determining critical heat flux during the boiling process, which is consistent with existing observations, but has not previously been specifically stated. The observed effects of the various geometric parameters of the porous coating on the critical heat flux, clearly illustrated by the capillary fluid flow inside the porous coating, play a significant role in the determination of critical heat flux. Currently available critical heat flux models were not found to accurately predict the test data in this study, primarily due to the aforementioned important factor.

Nomenclature

d_{pore}	=	pore size, μm
g	=	gravitational acceleration, m/s^2
h_{fg}	=	latent heat, kJ/kg
K_{cu}	=	copper thermal conductivity, W/mK
q''	=	heat flux, W/cm^2
R	=	bubble radius, mm
R_{br}	=	radius of breakthrough pore, μm
R_w	=	particle or wire radius of microporous coating, μm
r_m	=	tangential radius of liquid meniscus between a wire and wall, mm
TC	=	thermocouple
T_{sat}	=	liquid saturation temperature, K
$T_{\text{TC1–6}}$	=	temperature reading from thermocouple no. 1 to 6, K
T_w	=	wall temperature at bottom of capillary structure, K
t_{hole}	=	distance between two thermocouples, mm
t_{STC1}	=	distance between surface and thermocouple no.1, mm
t_w	=	porous coating thickness, mm

Greek Symbols

α	=	contact angle, deg
β_1	=	half open angle associated with wetting area, deg
β_2	=	half open angle associated with meniscus, deg
ε	=	volumetric porosity
λ_u	=	flow-critical length on uniform porous coating or wavelength, mm
ρ	=	density, kg/m^3
σ	=	surface tension, N/m

Subscripts

1–6	=	thermocouple number
l	=	liquid phase
u	=	uniform porous coating
v	=	vapor phase

I. Introduction

THE critical heat flux (CHF) defines the upper limit of boiling heat transfer and as a result, is one of the critical parameters governing the safety of boiling devices. Efforts have been made to enhance CHF as well as to better understand mechanisms which govern it. CHF has been found to be significantly improved through use of various porous coatings, which can be classified into two major categories: uniform or modulated sintered copper powders [1–5]; and metal or nonmetal flakes, foam or particles [6–11]. Enhancing CHF through use of porous coatings has been well recognized; however, the enhancement mechanisms responsible for this enhancement are not well understood. Several models [4,12–14] have been proposed to predict CHF in pool boiling on porous coatings, but these only apply for specific conditions. A universal model, which can explain the physics and predict the majority of the available test data on porous coatings with reasonable accuracy does not exist yet.

There are two principal questions, first, is CHF on porous coatings primarily caused by hydrodynamic instability? And what are the other factors that affect the enhancement? Polezhaev and Kovalev [14] found that the distance between the vapor-jet columns formed on uniformly porous coatings is approximately one-tenth of the Taylor critical wavelength for boiling on plain surfaces, and the number of vapor columns on porous coatings was greater than these on plain surfaces. Polezhaev and Kovalev [14] also believed that the porous structure rather than the Taylor instability is the decisive factor in the formation of the vapor columns for boiling on porous coatings. In order to maintain Helmholtz stability, higher vapor velocity is needed, which is also the primary cause of the enhanced CHF. Based on these analyses, Polezhaev and Kovalev [14] proposed an analytical expression to predict CHF on a uniform coated surface as

Presented at the Space Technology and Applications International Forum 2008, Albuquerque, NM, 10–14 February 2008; received 18 March 2008; revision received 24 January 2010; accepted for publication 31 January 2010.

*Assistant Professor, Department of Mechanical Engineering; Chen.Li@SC.EDU. Member AIAA (Corresponding Author).

†Professor and President, George W. Woodruff School of Mechanical Engineering. Fellow AIAA.

$$q''_{\mathrm{CHF}} = 0.52\varepsilon^{2.28} h_{fg} \sqrt{\sigma \rho_l \rho_v / (\rho_l + \rho_v) R_{\mathrm{br}}} \quad (1)$$

R_{br} is the radius of the vapor jets that break through the liquid. Experimental data for water, ethanol, and Freon-113 showed good agreement with the predictions of Eq. (1) [14]. By assuming $R_{\mathrm{br}} = R_w$, i.e., radius of the particle or wire of porous coatings, and $\rho_l/(\rho_l + \rho_v) \approx 1$, Liter and Kaviany [4] have rewritten Eq. (1) as

$$\frac{q''_{\mathrm{CHF}}}{(\pi/24)\rho_v^{0.5} h_{fg} [\sigma g(\rho_l - \rho_v)]^{0.25}} = \frac{3[\sigma g(\rho_l - \rho_v)]^{0.25}}{\lambda_u^{0.5}} \quad (2)$$

Where, $\lambda_u = 2R_w(\pi/5.88\varepsilon^{2.28})^2$ is the distance between vapor jets that flow from the surface (i.e., break though the liquid). λ_u is a function of geometry and structure only and independent of thermophysical properties. Use [4,14] for more details. The right hand side of Eq. (2) represents the ratio of the vapor film wavelength, i.e., the distance between vapor jets, on a plain surface to that on a porous coating. Equation (2) indicates that CHF could be enhanced if the wavelength of the vapor phase is reduced. Liter and Kaviany [4] demonstrated this principle for both dual-height modulation and single-height modulation where, through use of modulated porous surfaces, CHF was improved up to three times as compared with that of a similar plain surface. Liter and Kaviany [4] believed that CHF resulting from the modulation of a porous layer coating was primarily determined by the hydrodynamic limit. However, Malyshenko [5] and Borzenko and Malyshenko [2,3] found that the rate of propagation of the coating dryout front was approximately 10^{-2} cm/s and believed that CHF drying mechanism of pool boiling on porous coatings could not be fully explained or modeled by the hydrodynamic limit [4,14].

Clearly, the size of the particle/wire and the heated region both play important roles in the determination of CHF on porous coatings. Chang and You [7] found that CHF on diamond particles, Omegabond 101 epoxy, and alcohol, increased with particle size increase and was not sensitive to the thickness of the wick. Chang and You [7] believed that the enhancement of the active nucleation site density within the coating layer was the primary reason, due to the effective delay in the onset of film boiling. However, Borzenko and Malyshenko [3] demonstrated that for a given particle size, CHF strongly depended on both the thickness and particle size of the porous coating. The CHF was observed to increase with the decreasing heater size [15]. This is in part due to the vapor film, when formed on a smooth surface, being washed off by the powerful ascending currents of the liquid. Rainey and You [11] illustrated that this phenomena also exists for boiling on porous coated surfaces. While in the latter case, the porous material retards these currents, particularly as the size of the heated region increases. Additionally, liquid could be supplied from the sides for a smaller heated region, since the liquid flow path to the center of a smaller heater is shorter than that from a larger one.

O'Connor and You [9] and O'Connor et al. [10] observed numerous small bubbles (0.5–1.0 mm in diameter) adjacent to the enhanced surfaces, which is significantly different from the bubble behavior on plain surfaces. The large number of bubbles may be one of reasons for the improved CHF on porous coatings. Kim et al. [8] believed that the increased active nucleation site density helps prevent the bubbles from becoming too large prior to departure, resulting in higher bubble departure frequencies, which ultimately extend the nucleate boiling regime before hydrodynamic instability occurs. Variations in the contact angle may also be one of the factors enhancing CHF. Carey [16] proposed that surface conditions could greatly influence the contact angle and Chai and Wen [13] demonstrated this principle in both numerical and experimental studies. Their results indicated that the contact angle could be reduced through the application of a porous coating and hence CHF could be enhanced substantially.

The well known Zuber theory, which is shown here as Eq. (3), is the most widely accepted theory by which CHF on horizontal plain surfaces can be predicted [17]. The Zuber model indicates that CHF is independent of surface effects on plain surfaces:

$$q''_{\mathrm{CHF}} = \frac{\pi}{24} \rho_v^{1/2} h_{fg} [\sigma/(\rho_l + \rho_v)]^{1/4} \quad (3)$$

The preceding literature review illustrates two points: First that the prediction of CHF is not well understood, particularly as it pertains to porous surfaces, and second, that CHF can be substantially improved through the use of porous coated surfaces, but that the mechanisms for such enhancement are quite complicated and not well understood. It is clear, however, that CHF on a porous coating is strongly affected by some of the geometric parameters of the porous coating including the particle/wire, R_w, coating thickness, t_w, volumetric porosity, ε, and the size of the heated region (i.e., the heater size). In some cases, the existing models indicate the opposite effect of variations in some of these parameters, clearly indicating the need for additional study.

The primary objective of the current investigation is to better understand the dependent relationships between CHF and the geometric parameters of porous coatings by systematically examining the effects of these geometric parameters, including porous coating thickness, volumetric porosity, and pore size on CHF. In this study, the sintered pure copper woven mesh screens, which have highly controlled geometric parameters, were employed as microporous coatings.

II. Experimental Investigation

In this investigation, a series of experimental tests were conducted on horizontal, 8×8 mm thermally conductive porous coatings. Sintered pure copper woven mesh screens [18] were employed in order to carefully control the pore size, porosity, coating thickness, and wire size. The test article structure is shown as in Fig. 1. It consists of three components: an 8×8 mm square, multilayered sintered copper mesh section; a 0.03 mm thick copper foil; and an 8×8 mm square copper heating block with a 7.8 mm threaded cylindrical portion. Three thermocouples (TC_1, TC_2, and TC_3) are located at the center of the copper bar at 10 mm intervals. The

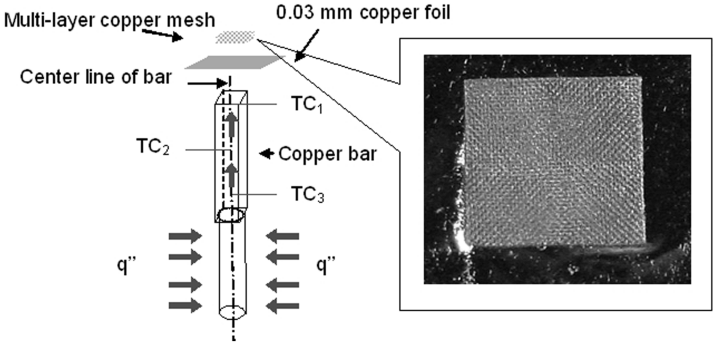

Fig. 1 a) Schematic of test setup for pool boiling [18] and b) the positions of three thermocouples in pool chamber.

Table 1 Specifications and CHF values of the test samples

Sample PB mesh no.-layer no.	Thickness, mm, t_w	Porosity, ε	Wire diameter, μm, $2R_w$	Pore size, μm, d_{pore}	CHF, W/cm^2
Porous coating thickness					
PB 145-2	0.21	0.737	56	119.2	176.1
PB 145-4	0.37	0.693	56	119.2	192.3
PB 145-6	0.57	0.701	56	119.2	221.9
PB 145-8	0.74	0.698	56	119.2	207.6
PB 145-16	1.38	0.69	56	119.2	337.2
PB 145-32	2.30	0.64	56	119.2	360.0
Volumetric porosity					
PB 145-4	0.37	0.693	56	119.2	192.3
PB 145-6c	0.36	0.56	56	119.2	193.7
PB 145-7c	0.37	0.409	56	119.2	192.2
Mesh size (mesh number and wire diameter)					
PB 145-4	0.37	0.693	56	119.2	192.3
PB 100-2	0.36	0.632	114	140	217.4
PB 60-1	0.38	0.67	191	232.2	330.1

temperature of the interface between the heating block and the wick structure can be derived from TC_1, which is located 0.5 mm below the porous-solid heating block interface.

The sintered copper woven mesh screen was directly sintered to the heating block to minimize the contact thermal resistance between the porous coating and the solid heating block [18]. The detailed fabrication procedure and sintering process can be found in [18]. The finished surface is shown in Fig. 1. A total of ten different test articles were evaluated experimentally. The specifications of these test articles are listed in Table 1 with the variables highlighted. The sample naming convention represents the porous coating structures characteristics; for example, PB145-6c denotes a pool boiling test sample that was fabricated from six layers of 5709 m^{-1} (145 in.$^{-1}$) copper woven mesh screen and compressed.

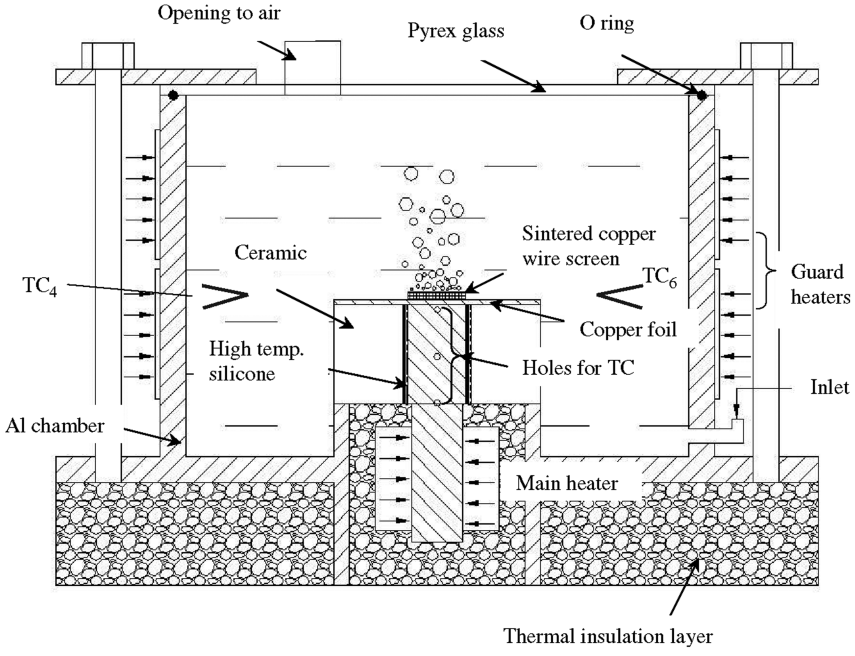

a)

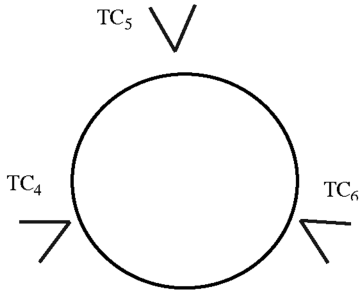

b)

Fig. 2 Schematic of test setup for pool boiling test [18].

Figure 2a illustrates the experimental test facility, the details of which can be found in [18]. The experimental test facility is composed of an aluminum (Al) chamber with two guard heaters, a reservoir for the distilled water supply, a heating system, and a data acquisition system. Nucleate boiling on a plain surface was used to calibrate the experimental test facility [19]. As shown in Fig. 2b, three K-type thermocouples (TC_4, TC_5, and TC_6) were used to monitor the water temperature at different locations. The test facility was allowed to reach steady-state, which is defined as the point at which the temperature reading for any thermocouple varied by less than 0.1°C over a period of ten minutes. Then the steady-state experimental data averaged over a period of five minutes were recorded at each power level. The power was then incremented and the process repeated, until CHF was reached.

The processes of data reduction and experimental uncertainties were identical to that described in [18]. The test data were categorized to obtain two metrics, computed from Eqs. (4) and (5), respectively, the superheat, $T_w - T_{\text{sat}}$, and the heat flux, q'', (including CHF):

$$T_W - T_{\text{sat}} = T_{\text{TC1}} - (T_{\text{TC4}} + T_{\text{TC5}} + T_{\text{TC6}})/3 - q'' t_{\text{STC1}}/K_{\text{cu}} \quad (4)$$

$$q'' = K_{\text{cu}}[(T_{\text{TC3}} - T_{\text{TC2}}) + (T_{\text{TC2}} - T_{\text{TC1}})]/2t_{\text{hole}} \quad (5)$$

In Eq. (4), $T_{\text{sat}} = (T_{\text{TC4}} + T_{\text{TC5}} + T_{\text{TC6}})/3$ and $T_W = T_{\text{TC1}} - q'' t_{\text{STC1}}/K_{\text{cu}}$. Here the terms T_{TC1}, T_{TC2}, and T_{TC3} denote the temperatures of the three K-type thermocouples used to monitor the axial temperature distribution in the copper heater at 10 mm intervals. Thermocouples T_{TC4}, T_{TC5}, and T_{TC6} were used to measure the water temperature in the test chamber. Using this measured temperature, T_{TC1}, and the known thermal conductivity, K_{cu}, the temperature at the bottom of the capillary wick structure (wall temperature), T_W, was derived. From this information, and using the known area, T_{TC1}, T_{TC2}, and T_{TC3}, the heat flux, q'', dissipated through evaporation/boiling under steady-state conditions, could be determined.

The uncertainty of the temperature measurements, the length (or width), and the mass are ±0.5°C, ±0.01 mm, and ±0.1 mg, respectively. A Monte Carlo propagation error simulation indicated the following 95% confidence level for the computed results: the heat flux was less than ±5.5 W/cm^2; the superheat ($T_w - T_{\text{sat}}$) was less than ±1.3°C, and the volumetric porosity, ε, was less than ±1.5%.

III. Results and Discussion

In order to systematically examine the effects of the main geometric parameters of the porous coatings on CHF, the porous coating thickness, t_w, the volumetric porosity, ε, and mesh size were varied from 0.21 to 2.3 mm, from 0.409 to 0.693, and from 2362 m^{-1} (60 in.$^{-1}$) to 5709 m^{-1} (145 in.$^{-1}$), respectively. The measured values of q''_{CHF} are summarized in Table 1.

A. Thickness Effects of the Conductive Microporous Coated Surfaces

In a number of tests, the porous coating thickness, t_w, was varied from 0.21 to 2.3 mm to assess its effect on CHF while the volumetric porosity, ε, and mesh size of the porous coating were held nearly constant. As shown in Fig. 3, dryout spots were not observed on the porous coating, which indicates that the whole porous coating was completely dried out in a very short time.

CHF is plotted as a function of the porous coating thickness, t_w, in Fig. 4. Note that heat fluxes on 1.38 and 2.30 mm thick porous/coated surfaces do not represent CHF values. They are instead, the highest heat fluxes that could be achieved during the tests prior to burnout, which resulted in destruction of the test article and prevented repeatability tests. CHF is believed to be higher than the documented heat flux for these two test articles. In another words, in these two particular cases, dryout was not approached because of the limitation of the heater power. Figure 4 illustrates that CHF initially increases with increasing porous coating thickness when the volumetric porosity and mesh size are held constant. The cause for CHF increases with increasing thickness of conductive porous coatings is believed to be the augmentation of the effective heat transfer area (actual heat flux in the liquid side is significantly reduced due to the fin effect introduced by the porous material), and the reduction in the flow resistance in the horizontal direction because of the increase of the flow area. From Fig. 4, the enhancement of CHF resulting from an effective heat transfer area augmentation appears to gradually fade when the porous coating thickness reaches a certain value, approximately 2 mm, in this study. In this type of porous material, the solid frame structure in a porous coating can be treated as fins and can be quantified fairly easily. The fin efficiency is likely to decrease with increasing porous coating thickness and thus the effective heat transfer area remains essentially unchanged. Additionally, with an increase in the thickness of the porous coating, the vapor flow resistance in the vertical direction will also increase substantially. This may result in difficulty in the liquid resupply and therefore implies an optimal thickness for CHF enhancement for a given volumetric porosity and wire size. Test results showed that for a porous coating thickness of less than 1 mm, CHF enhancement was approximately 30 ∼ 40% as compared with plain surfaces. However, when the porous coating thickness was greater than 1.4 mm, the highest heat flux enhancement achieved in this study was found to be an enhancement factor of two. Although wall dryout was not achieved, the wall superheat was observed to be significantly higher

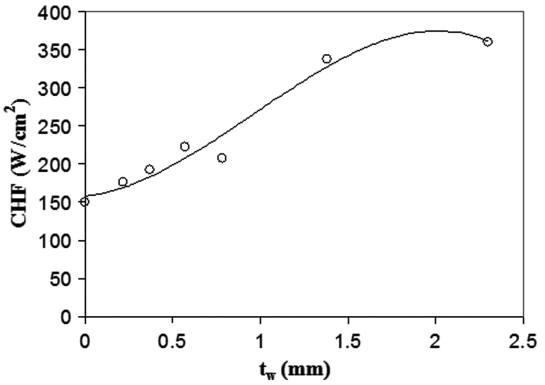

Fig. 4 CHF as a function of the porous coating thickness.

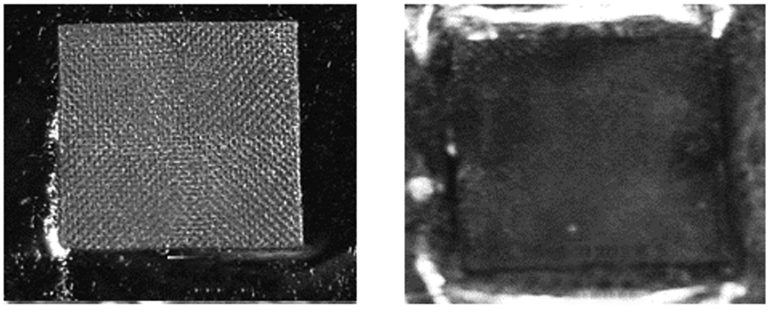

a) **b)**

Fig. 3 Pictures of finished sintered wire screen surface: a) before test and b) after dryout in present study.

than that on thin porous coatings, over a large range of heat fluxes [19]. Malyshenko [5] observed a similar phenomenon for thick, nonconductive porous coatings. As discussed in [19], this is believed to be mainly caused by the formation of a stable vapor film inside porous coatings, immediately adjacent to the heated surface. It was hypothesized that the mechanisms of CHF on thin porous coatings would be significantly different from that occurring for thick coatings although the definition of thick is not quantified.

The CHF on thin porous coatings is believed to occur during the transition from nucleate boiling to film boiling, and appears to be similar to the behavior occurring on plain surfaces. Figure 5 illustrates the characteristics of increasing wall superheat, as a function of time during dryout. It was found that the drying processes on porous coatings are nearly identical to that occurring on plain surfaces. Zuber [17] summarized and discussed the similarity between nucleate boiling and the flow of a gas bubbling through a porous surface, shown in detail in Sec. 3-4 of [17]. When combined with the new information presented here and as shown in Fig. 5, this indicates that the bubble behavior above the thin porous coatings is very similar to that occurring above plain surfaces.

Compared with nucleate boiling on a plain surface, the key differences between these two systems are the patterns and behavior of vapor/liquid phases inside the porous coatings. Vapor behavior inside a porous coating would significantly affect the distribution of the vapor stream leaving the surface of the porous coating. For the same heat flux input, the nucleate boiling process within a porous coating does not spread as readily as it does on a plain surface, and the vapor velocity leaving the porous coatings is higher due to the reduction of the active boiling area, which results in a constriction of the vapor stream as compared with that occurring on a plain surface. As shown in Fig. 6, Rainey and You [11] observed random bubble clusters on porous coatings instead of consistently alternating four- and five-bubble patterns, typical of plain surfaces. The film-boiling pattern was disturbed by vapor jets leaving the porous coatings, and thus enhancing CHF through porous coatings. Tehver [20] stated that CHF was enhanced on porous coatings because the time for replenishment of the liquid layer underneath the vapor mushroom was longer than that occurring on plain surfaces. In addition, the liquid supply is enhanced through the assistance of capillary pressure, which is generated from menisci formed at the liquid–vapor interfaces inside the porous coatings. The distribution of the vapor phase inside the porous coatings is of paramount importance in the determination of CHF and the boiling behavior on porous coatings. Further visualization study is needed to determine the vapor motion and the distribution of the vapor stream inside these porous coatings.

To evaluate the validity of the liquid replenishment model as described above, additional tests were conducted in which the edges of the porous coatings were sealed. This allowed the complex mechanisms controlling CHF on the thick porous coatings to be better understood. The results indicated that for both large and small porous coatings, sealing the sides of a porous coating resulted in a reduced

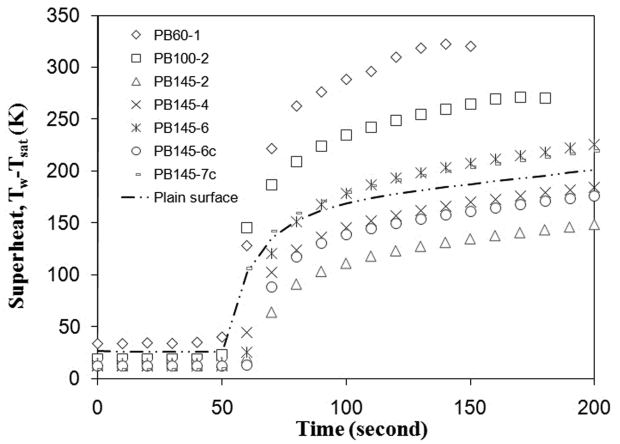

Fig. 5 Thermograms of wall superheat during the development of CHF on plain surfaces and porous coatings.

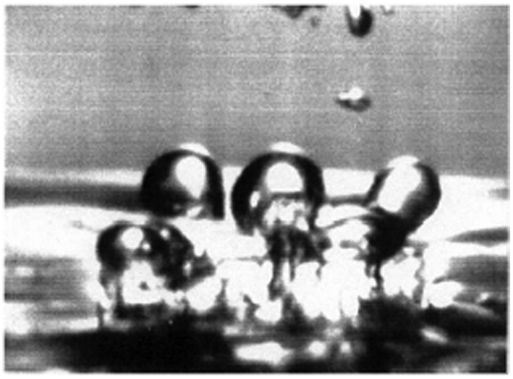

a)

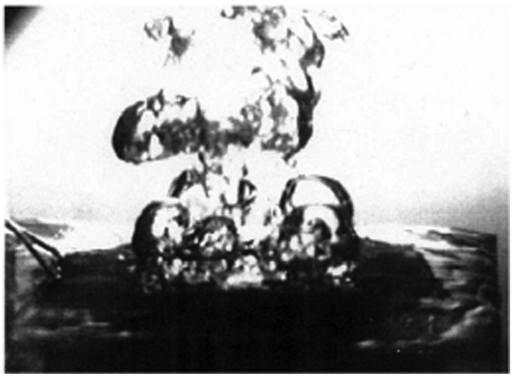

b)

Fig. 6 Photographs of CHF phenomenon for 4 cm^2 horizontal heater [11].

CHF as compared with that of a plain surface of similar size [4,21]. This confirms the liquid replenishment model presented here, in which liquid flows into the porous coating from the sides. Without the liquid replenishment mechanism, it is more difficult for the vapor to escape from porous coatings, which would result in high wall superheat. Generally, it has been recognized that the flow resistance is much higher through a wetted porous coating than through a dry porous coating [22]. Additionally the vapor flow length becomes longer due to the flow crimping when the porous coatings are thicker [23].

However, if all sides of the porous coatings remain open, CHF is found to be greatly enhanced because of three factors: the small size effect [11], the capillary driven rewetting effects [4], and the ability of the vapor to escape and be replenished by liquid from the sides [24]. For the case of coatings unsealed on the sides, nucleate boiling occurs in porous coatings and evaporation happens at the liquid–vapor interface inside the porous coatings. Liquid is generally supplied from above with the assistance of capillary pressure. Vapor primarily escapes through the dry passage, which is formed between the liquid–vapor interfaces inside the porous coatings during the boiling process. Vapor film thickness increases with increasing heat flux, and finally equals or exceeds the thickness of a porous coating itself, which therefore leads to surface dryout, i.e., CHF [19]. The mechanism in determining CHF for this situation is a combination of the capillary limit inside the porous coating and the hydraulic flow resistance limit occurring inside the porous coatings.

B. Effects of Mesh Size of the Conductive Microporous Coated Surfaces

In this section, the volumetric porosity, ε, and thickness of the conductive porous coatings t_w, were held constant, and the mesh size was varied to evaluate its effect on CHF. It shall be noted here that the pore size, d_{pore}, and wire diameter, $2R_w$, are also varied with the change of the mesh size.

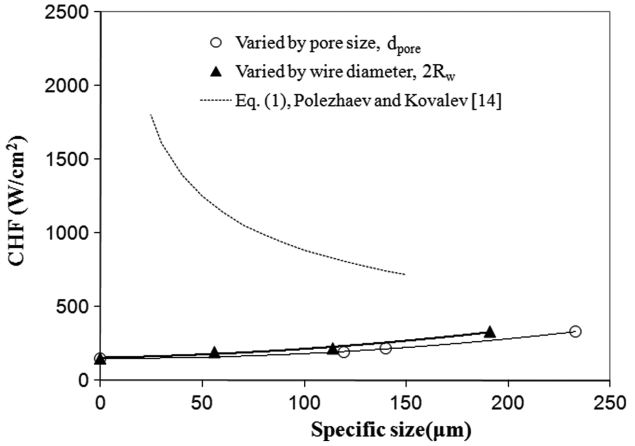

Fig. 7 CHF as a function of specific size of porous coatings such as pore size and wire diameter.

In Fig. 7, CHF is presented as a function of the pore size, d_{pore}, or wire diameter, $2R_w$. For comparison, the prediction of the Polezhaev and Kovalev model [14] is shown in Fig. 7. It is very hard to explain why CHF increases with increasing pore size for a given volumetric porosity and porous coating thickness. However, plausible reasons can be found to explain CHF increase with increasing wire diameter for a given volumetric porosity and thickness, which is consistent with the observations of Chang and You [7] as well as those of Hwang and Kaviany [25]. These two independent studies [7,25] observed a CHF increase with a corresponding increase in the particle size, but the explanations were not provided in these studies. A possible explanation of this phenomenon is the existence of the capillary evaporation inside the porous coatings at pre-CHF, i.e., the presence of menisci between the wire/particle and the wall. This observation may be similar to what Li et al. [18] found in capillary evaporation. As shown in Fig. 8, the reason that CHF increases with increasing wire or particle size may be due to the change in the meniscus radius, r_m, which gets smaller with a larger size wire radius, R_w, when compared with that for smaller particles/wires at the same flow resistance [18]. Alternatively, the induced capillary pressure is higher in the space formed between the larger size wire/particle and the heated wall than the pressure occurring between the smaller particles/wires and the wall at a given flow rate. This finding implies that capillary fluid flow inside the porous coating plays an important role in governing CHF on porous coatings. As shown in Eq. (1), Polezhaev and Kovalev's model [14] considered the surface pore size as one of major factors in determining CHF on a porous coating, which is similar to the capillary limit on evaporation. However, the term that represents the capillary effect inside a porous coating was missing from the Polezhaev and Kovalev model [14], which is the state-of-the-art CHF model on a porous coating. Actually, the capillary effect on CHF inside porous coatings was not considered in all available CHF models [4,12–14]. In Fig. 7, it was shown that the Polezhaev and Kovalev model [14] fails to accurately predict this effect. Figure 7 also illustrates that CHF on a porous coating is not caused by the capillary limit at the surface of a porous coating, but clearly by capillary flow inside the porous coatings, which has been found to be very important and needs to be seriously considered in any future CHF models.

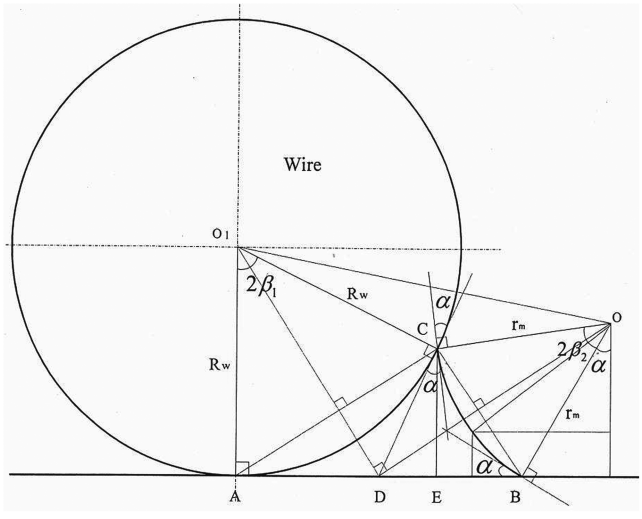

Fig. 8 Schematic of the meniscus between the wire and the wall [26].

C. Effects of Volumetric Porosity of the Conductive Microporous Coated Surfaces

In the current investigation, the volumetric porosity, ε, was varied from 0.409 to 0.693 in order to examine its effect on CHF for a given coating thickness, t_w, and mesh size. CHF is plotted in Fig. 9 as a function of volumetric porosity. Here, CHF on a plain surface was assumed to be evaluated at a volumetric porosity of $\varepsilon = 0$ or 1. The prediction of the Polezhaev and Kovalev model [14] is also shown in Fig. 9 for comparison.

Figure 9 clearly indicates the existence of an optimal volumetric porosity for CHF if the coating thickness and mesh size of the porous coatings are given. As indicted in [19], only the vertical pore size was changed in this experimental study. Test data illustrated that CHF was dependent on this parameter, which hints that the menisci could be formed between the wires in the vertical direction, and as a result, the capillary flow plays an important role in the enhancement of the liquid supply. Hence, it could be expected that in the liquid supply process, the liquid is fed into the porous coatings by gravitational and capillary forces, and then spreads horizontally to the sites from which the bubbles depart. Therefore, as the capillary force increases with decreasing pore size, the liquid flow resistance increases at the same time. As a result, there is a tradeoff between these two factors, which provides the best improvement in CHF.

Figure 9 illustrates the effect of capillary fluid flow inside the porous coatings on CHF. None of the previous CHF modeling approaches [4,12–14] considers this type of capillary flow condition. As shown in Eq. (1), the Polazhaev and Kovalev model [14] indicates that CHF would always increase with increasing volumetric porosity, which does not make much sense physically even without considering the capillary fluid flow inside the porous coatings. With the reduction of heat transfer area and fin efficiency, CHF is likely to be lower on a very highly porous surface as compared with that for a moderately porous surface, if assuming an identical porous structure. From Fig. 9, the Polazhaev and Kovalev model [14] gives a lower prediction when the volumetric porosity, ε, is less than 0.3, while this model shows much higher predictions when ε is larger than 0.3. In short, the Polazhaev and Kovalev model is not able to predict the experimental data accurately since the capillary fluid flow, which were found to affect the vapor stream flow pattern leaving the porous

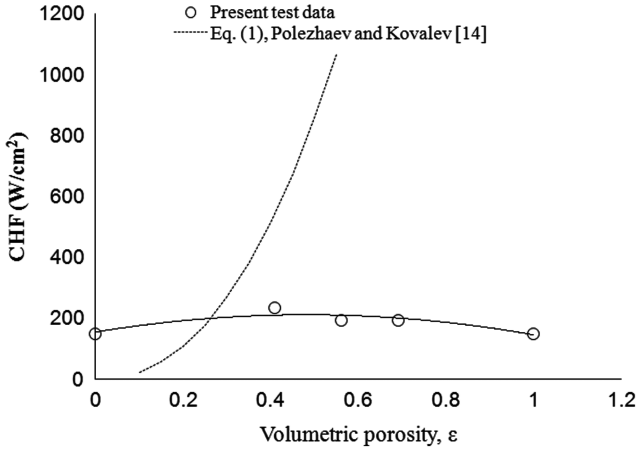

Fig. 9 CHF as a function of volumetric porosity of porous coatings.

coatings, have not been included. Combining is the discussion with that in the previous section, this experimental study strongly illustrates that the capillary fluid flow inside the porous coatings affects CHF substantially.

IV. Conclusions

The effects of the principal geometric parameters such as coating thickness, volumetric porosity and mesh size of horizontal microporous coatings made from sintered woven mesh on CHF were systematically examined in this experimental study. The results indicate that CHF increases with increasing coating thickness, but also strongly suggests that there is a critical coating thickness that distinguishes CHF mechanism between thick and thin porous coatings. The CHF mechanism on the thin porous coatings appears to be primarily governed by the hydraulic instability resulting from the surfaces of the porous coatings; while CHF mechanism for the thick porous coatings with open sides is from a combination of the capillary limit resulting from the capillary flow inside the porous coatings and the hydraulic instability resulting from surface variations in the porous coatings.

The dependence of CHF on the wire size also indicates that capillary evaporation occurs pre-CHF. The existence of an optimal volumetric porosity for CHF is believed to be primarily determined by the tradeoff between the capillary pressure induced inside the porous coatings and the liquid flow resistance. The combined effects of the geometric parameters on CHF, strongly indicates that the capillary fluid flow inside the porous coatings is part of the major factors that determinate CHF for nucleate boiling on porous coatings.

The capillary evaporation inside porous coatings may be one of the most important factors by which CHF on porous coatings can be enhanced. In short, the augmentation of the active nucleate site density, intensified convection by liquid–vapor counter flow and the assistance of liquid supply through the capillary pressure generated inside the porous coatings, may be the major factors contributing to the improvement of CHF and determining CHF in these types of porous coatings. The state-of-the-art CHF models of porous coatings were not found to accurately predict the available test data. This is because these models do not take into account the capillary fluid flow inside the porous coatings, which is clearly a major factor in the determination of CHF for these porous coatings.

Acknowledgment

The authors would like to acknowledge the support of the National Science Foundation under award CTS-0312848.

References

[1] Bergles, A. E., and Chyu, M. C., "Characteristics of Nucleate Pool Boiling from Porous Metallic Coatings," *Journal of Heat Transfer*, Vol. 104, No. 2, 1982, pp. 279–285. doi:10.1115/1.3245084

[2] Borzenko, V. I., and Malyshenko, S. P., "Experimental Research of Heat Transfer Enhancement and Thermal Stability at Pool Boiling on Porous Surfaces," *4th World Conference of Experimental Heat Transfer, Fluid Mechanics and Thermodynamics*, Brussels, Belgium, 1997, Paper HT-RU-21.

[3] Borzenko, V. I., and Malyshenko, S. P., "Mechanisms of Phase Exchange Under Conditions of Boiling on Surfaces with Porous Coating," *High Temperature*, Vol. 39, No. 5, 2001, pp. 769–776.

[4] Liter, S. G., and Kaviany, M., "Pool-Boiling CHF Enhancement by Modulated Porous-Layer Coating: Theory and Experiment," *International Journal of Heat and Mass Transfer*, Vol. 44, No. 22, 2001, pp. 4287–4311. doi:10.1016/S0017-9310(01)00084-9

[5] Malyshenko, S. P., "Characteristics of Heat Transfer with Boiling on Surfaces with Porous Coatings," *Thermal Engineering [Translation of Teploenergetika (Moscow)]*, Vol. 38, No. 2, 1991, pp. 81–88.

[6] Chang, J. Y., You, S. M., and Haji-Sheikh, A., "Film Boiling Incipience at the Departure from Natural Convection on Flat Smooth Surfaces," *Journal of Heat Transfer*, Vol. 120, No. 2, 1998, pp. 402–409. doi:10.1115/1.2824264

[7] Chang, J. Y., and You, S. M., "Boiling Heat Transfer Phenomena from Micro Porous and Porous Surfaces in Saturated FC-72," *International Journal of Heat and Mass Transfer*, Vol. 40, No. 18, 1997, pp. 4437–4447. doi:10.1016/S0017-9310(97)00055-0

[8] Kim, J. H., Rainey, K. N., You, S. M., and Pak, J. Y., "Mechanism of Nucleate Boiling Heat Transfer Enhancement from Microporous Surface in Saturated FC-72," *Journal of Heat Transfer*, Vol. 124, No. 3, 2002, pp. 500–506. doi:10.1115/1.1469548

[9] O'Connor, J. P., and You, S. M., "A Painting Technique to Enhance Pool Boiling Heat Transfer in Saturated FC-72," *Journal of Heat Transfer*, Vol. 117, No. 2, 1995, pp. 387–393. doi:10.1115/1.2822534

[10] O'Connor, J. P., and You, S. M., and Price, D. C., "Thermal Management of High Power Microelectronics via Immersion Cooling," *IEEE Transactions on Components, Packaging, and Manufacturing Technology*, Vol. 18, No. 3, 1995, pp. 656–663. doi:10.1109/95.465166

[11] Rainey, K. N., and You, S. M., "Effects of Heat Size and Orientation on Pool Boiling Heat Transfer from Microporous Coated Surfaces," *International Journal of Heat and Mass Transfer*, Vol. 44, No. 14, 2001, pp. 2589–2599. doi:10.1016/S0017-9310(00)00318-5

[12] Barthelemy, R. R., "Evaporation Heat Transfer in Heat Pipes," *2nd International Heat Pipe Conference*, Bolgana, Italy, 1976, pp. 425–436.

[13] Chai, L. H., and Wen, D. S., "Theoretical Analyses on Boiling Critical Heat Flux with Porous Media," *Heat and Mass Transfer*, Vol. 41, No. 9, 2005, pp. 780–784. doi:10.1007/s00231-004-0610-9

[14] Polezhaev, Y. V., and Kovalev, S. A., "Modeling Heat Transfer with Boiling on Porous Structures," *Thermal Engineering [Translation of Teploenergetika (Moscow)]*, Vol. 37, No. 12, 1990, pp. 617–620.

[15] Kudritskiy, G. R., "Heat Transfer Intensity and Critical Heat Flux Densities in Boiling of Liquid on a Microsurface," *Heat Transfer: Soviet Research*, Vol. 18, No. 3, 1986, pp. 65–69.

[16] Carey, V. P., *Liquid-Vapor Phase Change Phenomena*, Hemisphere, New York, 1992.

[17] Zuber, N., "Hydrodynamic Aspects of Boiling Heat Transfer," AEC Rept. AECU-4439, Physics and Mathematics, 1959.

[18] Li, C., Peterson, G. P., and Wang, Y. X., "Evaporation/Boiling on Thin Capillary Wick, 1: Thickness Effects," *Journal of Heat Transfer*, Vol. 128, No. 12, 2006, pp. 1312–1319. doi:10.1115/1.2349507.

[19] Li, C., and Peterson, G. P., "Parametric Study on Boiling Performance and Feature for Pool Boiling on Horizontal Conductive Micro Porous Coated Surfaces," *Journal of Heat Transfer*, Vol. 129, No. 11, 2007, pp. 1465–1475. doi:10.1115/1.2759969

[20] Tehver, J., "Influences of Porous Coating on the Boiling Burnout Heat Flux," *Recent Advance in Heat Transfer: Proceedings of the First Baltic Heat Transfer Conference*, Goteborg, Sweden, 1992, pp. 231–242.

[21] Udell, K. S., "Heat Transfer in Porous Media Considering Phase Change and Capillarity: The Heat Pipe Effect," *International Journal of Heat and Mass Transfer*, Vol. 28, No. 2, 1985, pp. 485–495. doi:10.1016/0017-9310(85)90082-1

[22] Cornwell, K., Nair, B. G., and Patten, T. D., "Observation of Boiling in Porous Media," *International Journal of Heat and Mass Transfer*, Vol. 19, No. 2, 1976, pp. 236–238. doi:10.1016/0017-9310(76)90121-6

[23] Semenic, T., Lin, Y. Y., and Catton, I., "Biporous Sintered Copper for a Closed Loop Heat Pipe Evaporator," *ASME Proceedings of IMECE*, IMECE Paper 2005-82180, Orlando, FL, 2005.

[24] Moss, R. A., and Kelly, A. J., "Neutron Radiographic Study of Limiting Planar Heat Pipe Performance," *International Journal of Heat and Mass Transfer*, Vol. 13, No. 3, 1970, pp. 491–502. doi:10.1016/0017-9310(70)90145-6

[25] Hwang, G. S., and Kaviany, M., "Critical Heat Flux in Thin, Uniform Particle Coatings," *International Journal of Heat and Mass Transfer*, Vol. 49, Nos. 5–6, 2006, pp. 844–849. doi:10.1016/j.ijheatmasstransfer.2005.09.020

[26] Yaxiong, W., "The Theoretical Analysis and Experimental Investigation of a Flexible, Lightweight Radiator with Micro Heat Pipe," Ph.D. Dissertation, Texas A and M Univ., College Station, TX, 2001.